

Cluster-decay of hot $^{56}\text{Ni}^*$ formed in $^{32}\text{S} + ^{24}\text{Mg}$ reaction

Raj K. Gupta^{a,b,c}, Rajesh Kumar^a, Narinder K. Dhiman^a, M. Balasubramaniam^{a,b}, Werner Scheid^b and C. Beck^c

^a *Physics Department, Panjab University, Chandigarh-160014, India.*

^b *Institut für Theoretische Physik, Justus-Liebig-Universität,
Heinrich-Buff-Ring 16, D-35392, Giessen, Germany.*

^c *Institut de Recherches Subatomiques, UMR7500, IN2P3/ Université
Louis Pasteur, F-67037 Strasbourg, France.*

(November 2, 2018)

The decay of $^{56}\text{Ni}^*$, formed in $^{32}\text{S} + ^{24}\text{Mg}$ reaction at the incident energies $E_{cm}=51.6$ and 60.5 MeV, is calculated as a cluster decay process within the Preformed Cluster-decay Model (PCM) of Gupta et al. re-formulated for hot compound systems. Interesting enough, the cluster decay process is shown to contain the complete structure of both the measured fragment cross sections and total kinetic energies (TKEs). The observed deformed shapes of the exit channel fragments are simulated by introducing the neck-length parameter at the scission configuration, which nearly coincides the ^{56}Ni saddle configuration. This is the only parameter of the model, which though is also defined in terms of the binding energy of the hot compound system and the ground-state binding energies of the various emitted fragments. For the temperature effects included in shell corrections only, the normalized α -nucleus s-wave cross sections calculated for nuclear shapes with outgoing fragments separated within nuclear proximity limit (here ~ 0.3 fm) can be compared with the experimental data, and the TKEs are found to be in reasonably good agreement with experiments for the angular momentum effects added in the sticking limit for the moment of inertia. The incident energy effects are also shown in predicting different separation distances and angular momentum values for the best fit. Also, some light particle production (other than the evaporation residue, not treated here) is predicted at these energies and, interestingly, ^4He , which belongs to evaporation residue, is found missing as a dynamical cluster-decay fragment. Similar results are obtained for temperature effects included in all the terms of the potential energy. The non- α fragments are now equally important and hence present a more realistic situation with respect to experiments.

PACS Nos. 25.70.Jj, 23.70.+j, 24.10.-i, 23.60.+e

I. INTRODUCTION

Experimentally, ^{56}Ni is an extensively studied compound system by using different entrance channels, namely $^{16}\text{O} + ^{40}\text{Ca}$, $^{28}\text{Si} + ^{28}\text{Si}$ and $^{32}\text{S} + ^{24}\text{Mg}$, and at various incident energies ranging from 1.5 to 2.2 times the Coulomb barrier (see, e.g., the review [1] and the other direct and more recent Refs. [2–8]). At such incident energies, the incident flux is found to get trapped by the formation of a compound nucleus (CN), which is in addition to a significant large-angle elastic scattering cross section. For lighter masses ($A_{CN} < 44$), such a compound nucleus decays subsequently by the emission of mainly light particles (n, p, α) and γ -rays; i.e. with very small component of heavy fragment ($A > 4$) emission. An experimental measure of this so-called particle evaporation residue yield is the CN fusion cross section. For somewhat heavier systems, like ^{48}Cr and ^{56}Ni , a significant decay strength to $A > 4$ fragments, the mass-asymmetric channels, is also observed which could apparently not arise from a direct reaction mechanism because of the large mass-asymmetry differences between the entrance and exit channels. The measured angular distributions and energy spectra are consistent with fission-like decays of the respective compound systems.

For the $^{32}\text{S} + ^{24}\text{Mg} \rightarrow ^{56}\text{Ni}^*$ reaction, in one of the experiments, the mass spectra for $A=12$ to 28 fragments and the total kinetic energy (TKE) for only the most favoured (enhanced yields) α -nucleus fragments are measured at the energies $E_{lab} = 121.1$ and 141.8 MeV, or equivalently at $E_{cm} = 51.6$ and 60.5 MeV, respectively [2,3]. Note that ^{56}Ni is a negative Q-value system (negative Q_{out} , different for different exit channels) and hence would decay only if it were produced in heavy ion reactions with sufficient compound nucleus excitation energy E_{CN}^* ($= E_{cm} + Q_{in}$), to compensate for the negative Q_{out} , the deformation energy of fragments E_d , their total kinetic energy TKE and the total excitation energy TXE, in the exit channel, as

$$E_{CN}^* = |Q_{out}(T)| + E_d(T) + TKE(T) + TXE(T); \quad (1)$$

see Fig.1 where E_d is neglected because fragments are considered to be spherical. Here Q_{in} is positive ($=16.68$ MeV for $^{32}\text{S} + ^{24}\text{Mg}$ entrance channel) and hence adds to the entrance channel kinetic energy E_{cm} of the two incoming nuclei in their ground states. In another experiment [4] for $^{32}\text{S} + ^{24}\text{Mg}$ reaction at $E_{cm} = 51.0$ and 54.5 MeV, the excitation-energy spectra for only the symmetric $^{28}\text{Si} + ^{28}\text{Si}$ and near-symmetric $^{24}\text{Mg} + ^{32}\text{S}$ channels are measured,

whose analysis indicate that a specific set of states in ^{28}Si correspond to highly deformed bands. In other words, the expected shapes of some of the observed fragments in the exit channel could be relatively deformed. It is interesting to note that this result is supported by a very recent study of the $^{28}Si + ^{28}Si$ reaction at $E_{cm} = 55$ MeV, where the population of highly excited states in the ^{24}Mg , ^{28}Si and ^{32}S nuclei indicated a selective and enhanced population of deformed bands [6]. In a still other recent experiment [7], the incident energy used in the same $^{32}S + ^{24}Mg \rightarrow ^{56}Ni^*$ reaction is $E_{lab} = 130$ MeV and an enhanced emission yield by a factor of 1.5 to 1.8 is observed for 8Be over the two α -particles. The aim of our present work is to understand some of the results of these experiments.

The above stated light particles ($A \leq 4$) production, the evaporation residue, is very satisfactorily understood as the equilibrated compound nucleus emission in the statistical Hauser Feshbach analysis [3,9–12], using the LILITA or CASCADE codes. The Hauser Feshbach calculations are also extended to include the complex fragments, like the ones observed in the experiments mentioned above. These are considered in the, so-called, BUSCO code [10] or the Extended Hauser-Feshbach scission-point model [12]. Within the framework of the Extended Hauser-Feshbach method [12], the above noted observed enhanced emission of 8Be over the evaporation of two α -particles in $^{32}S + ^{24}Mg$ reaction is shown related to an increased deformation of the heavier fragment ^{48}Cr [7]. The emission of complex fragments ($A > 4$, also called the intermediate mass fragments, IMFs, or "clusters") is alternatively treated as the binary fission of a compound nucleus in the statistical fission models [13,14], using the GEMINI code [9] or the saddle-point "transition-state" model [3,5,11]. The transition-state model, treating the complex fragments emission as a compound-nucleus fission process (the fusion-fission) seems to explain the observed mass spectra and excitation-energy spectra rather well for the $^{32}S + ^{24}Mg$ reaction at the two energies used in respective experiments [3,4]. Also, the measured TKE for the symmetric fission is comparable to the saddle-point potential energy at $\ell = 36\hbar$ [3]. Then, there are other processes, like the deep-inelastic (DI) orbiting or scattering, that have also been studied for this reaction but do not seem to explain the observed data [3].

In the statistical fission models [13,14], the fission decay of a compound nucleus is determined by the phase space (level density) available at the "transition" configuration, which is saddle or scission in these models. For light systems, this choice can lead to a significant population of many energetically allowed mass channels, though there is no structure information of the compound system in these fission models. However, the structure effects of the compound system seem to influence the observed yields strongly since strong resonance behaviour is observed in the measured excitation functions of large-angle elastic and inelastic scattering yields in several light systems (see, e.g., [6]). One possibility to account for such structure effects is via the process of fragments (or clusters) preformation in a compound nucleus and its subsequent decay as a cluster decay process, proposed recently by some of us [15,16]. The structure information enters the process via the preformation probability (also, known as the spectroscopic factors) of the fragments. We follow this approach of preformed cluster decay [15,16] here in this paper.

The cluster decay process was recently studied [15] for the compound system $^{56}Ni^*$, using the preformed cluster-decay model (PCM) of Gupta and collaborators [17–21]. It was shown that for the decay of $^{56}Ni^*$, the two processes of binary fission (the dynamical collective mass transfer calculated, by some of us [22–25], in the quantum mechanical fragmentation theory [26–28]) and cluster decay are almost indistinguishable, particularly at higher angular momenta. However, this work was a simple model study where the role of TKE was analysed and found to be significant for α -nucleus structure in the measured yields. This model is more recently re-formulated [16] for the IMFs emitted from an excited $^{116}Ba^*$ compound nucleus produced in low energy $^{58}Ni + ^{58}Ni$ reaction. The IMFs in $^{116}Ba^*$ are shown to be produced as multiple "clusters" of masses $A < 20$ and only at $E_{lab} > 200$ MeV, in agreement with experiments. Both of these works [15,16] show that the IMFs in decay of excited $^{116}Ba^*$ or the complete mass spectra in decay of excited $^{56}Ni^*$ have their origin in the macroscopic liquid drop energy (the shell effects are almost zero at the excitation energies involved). For $^{116}Ba^*$ decay, the light particles ($Z \leq 2$) emission, other than the promptly emitted via the statistical evaporation process (not treated in this model), is also shown to be given, but at higher energies where only the pure liquid drop energies enter the calculations. Thus, the macroscopic liquid drop energy (V_{LDM}) is shown playing the most important role in the cluster decay calculations. Apparently, the compound nucleus being hot at the energies involved, the V_{LDM} should also depend on the temperature T . This is done here in this paper for the decay of $^{56}Ni^*$ formed in $^{32}S + ^{24}Mg$ reaction at the two energies, $E_{cm} = 51.6$ and 60.5 MeV [2,3]. Also, the other terms of the potential, that constitute the scattering potential $V(R)$, are considered T -dependent.

The T -dependent liquid drop model used is that of Davidson et al. [29] which is based on the semi-empirical mass formula of Seeger [30]. The model parameters of Seeger's formula at $T=0$ are re-fitted in view of the present availability of a larger data set for binding energies [31]. For the T -dependence in $V(R)$, we follow Davidson et al. [29] and some other authors [32], discussed below. The deformation effects of the fragments (and the neck formation between them) are included here within the extended model of Gupta and collaborators [33–35], via a neck-length parameter at the scission configuration which simulates the two centre nuclear shape parametrization, used for both the light and heavy nuclear systems. A similar method has been used earlier by other authors [3,11,12], discussed below.

The dynamical cluster decay model for hot compound systems, a re-formulation of the preformed cluster-decay model (PCM) of Gupta and co-workers [17–21] for ground-state decays, is presented in section 2 and its application

to the hot $^{56}\text{Ni}^*$ nucleus data from Refs. [2,3] in section 3. The (statistical) evaporation of light particles, that occur promptly before the beginning of the binary decay process of cluster emission studied here, is not included in this paper. Hence, any discussion of light particles emission is that of one which is in addition to the ones emitted promptly. Finally, a summary of our results is presented in section 4.

II. THE DYNAMICAL CLUSTER DECAY MODEL FOR HOT COMPOUND SYSTEMS

The cluster decay model developed here is the preformed cluster-decay model (PCM) of Gupta et al. [17–21] for the ground-state decays, re-formulated for hot and excited compound systems. In this model, we treat the complex fragments (the IMFs or clusters) as dynamical collective mass motion of preformed fragments through the barrier. It is based on the well known dynamical (or quantum mechanical) fragmentation theory [26–28] developed for fission and heavy ion reactions, and used later for predicting the exotic cluster radioactivity [36–38] also. This theory is worked out in terms of the collective coordinates of mass asymmetry $\eta = (A_1 - A_2)/(A_1 + A_2)$ and relative separation R, which in a PCM allows to define the decay half-life $T_{\frac{1}{2}}$, or the decay constant λ , as

$$\lambda = \frac{\ln 2}{T_{\frac{1}{2}}} = P_0 \nu_0 P, \quad (2)$$

where P_0 , the preformation probability, refers to η -motion and P, the penetrability, to R-motion. Apparently, the two motions are taken as decoupled, an assumption justified in our earlier works [26,27,39]. The ν_0 is the barrier assault frequency. In terms of the partial waves, the decay cross section

$$\sigma = \frac{\pi}{k^2} \sum_{\ell=0}^{\ell_c} (2\ell + 1) P_0 P; \quad k = \sqrt{\frac{2\mu E_{c.m.}}{\hbar^2}} \quad (3)$$

with $\mu = [A_1 A_2 / (A_1 + A_2)] m = \frac{1}{4} A m (1 - \eta^2)$ as the reduced mass and ℓ_c , the critical (maximum) angular momentum, defined later. m is the nucleon mass. This means that λ in (2) gives the s-wave cross section, with a normalization constant ν_0 , instead of the π/k^2 in (3). However, in the present calculations, made for $\ell = 0$ case, the normalization constant is obtained empirically from the experimental data.

For η -motion, we solve the stationary Schrödinger equation in η , at a fixed R,

$$\left\{ -\frac{\hbar^2}{2\sqrt{B_{\eta\eta}}} \frac{\partial}{\partial \eta} \frac{1}{\sqrt{B_{\eta\eta}}} \frac{\partial}{\partial \eta} + V_R(\eta, T) \right\} \psi^\nu(\eta) = E^\nu \psi^\nu(\eta), \quad (4)$$

with $\nu=0,1,2,3\dots$ and $R = R_a = C_t (= C_1 + C_2)$, the first turning point, fixed empirically for the ground-state ($T=0$) decay since this value of R (instead of the compound nucleus radius R_0) assimilates to a good extent the effects of both the deformations β_i of two fragments and neck formation between them [35]. In other words, the deformation effects of the two fragments are included here in the scattering potential $V(R, T=0)$ for each η by raising the first turning point R_a from $R_a = R_0$ to $R_a = C_t$ or $C_t + \sum \delta R(\beta_i)$, which is equivalent of lowering of the barrier, as is found to be the case for deformed fragments [35]. This method of inclusion of fragment deformation and the parametrization of the neck zone via a neck-length parameter δR in the present calculations is quite similar to what has been achieved in both the transition-state model of Sanders [3,11] (in saddle point configuration) and the Extended Hauser-Feshbach Method of Matsuse and collaborators [12] (in scission point configuration). It is also shown in [35] that the alternative of calculating the fragmentation potential $V(\eta)$ and scattering potential $V(R)$ for deformed nuclei is not practical since the experimental deformation parameters for all the possible fragments (A_1, A_2), required for calculating $V(\eta)$, are generally not available. The deformation effects of nuclei in our calculations are further included via the Süssmann central radii $C_i = R_i - (b/R_i)$, with the radii $R_i = 1.28 A_i^{1/3} - 0.76 + 0.8 A_i^{-1/3} \text{ fm}$ and surface thickness parameter $b = 0.99 \text{ fm}$. Note that the C_t are different for different η -values and hence C_t is $C_t(\eta)$.

The eigen-solutions of Eq. (4) give the preformation probability

$$P_0 = \sqrt{B_{\eta\eta}} | \psi(\eta(A_i)) |^2 (2/A), \quad (5)$$

($i=1$ or 2), where $\psi(\eta)$ is $\psi^{\nu=0}(\eta)$ if the ground-state solution is chosen. However, the decay of ^{56}Ni in the ground-state ($T=0, R_a = C_t$) is not allowed since $Q_{out}(T=0)$ is negative.

For the decay of a hot compound nucleus, we use an ansatz [16] for the first turning point,

$$R_a = C_t(\eta, T) + \Delta R(\eta, T), \quad (6)$$

which depends on the total kinetic energy $TKE(T)$. The corresponding potential $V(R_a)$ acts like an effective, positive Q-value, Q_{eff} , for the decay of the hot compound system at temperature T to two fragments in the exit channel observed in the ground-states ($T=0$). Thus, in terms of the respective binding energies B , Q_{eff} is defined as

$$\begin{aligned} Q_{eff}(T) &= B(T) - [B_1(T=0) + B_2(T=0)] \\ &= TKE(T) \\ &= V(R_a). \end{aligned} \quad (7)$$

Since, $R_a = C_t(\eta)$ for $T=0$, $\Delta R(\eta)$ corresponds to the change in TKE at T with respect to its value at $T=0$ and hence can be estimated exactly for the temperature effects included in the scattering potential $V(R)$. Note that in Eq. (6) C_t is also taken to depend on temperature, as is defined later in the following. Also, ΔR depends on η . In the following, however, based on our earlier work [16], instead, we use a constant average value $\overline{\Delta R}$, independent of η , which also takes care of the additional $\sum \delta R(\beta_i)$ effects of the deformations of fragments and neck formation between them. Note that $\overline{\Delta R}$ is the only parameter of the model, though it is shown that the structure of the calculated mass spectrum is nearly independent of the exact choice of this parameter value. The corresponding Q_{eff} is denoted as $Q_{eff}(\overline{\Delta R})$.

In the above definition of Q_{eff} , apparently the two fragments would come out of the barrier and go to ground state ($T \rightarrow 0$) only by emitting some light particle(s) and/or γ -rays of energy, defined as (see Fig. 8)

$$\begin{aligned} E_x &= B(T) - B(0) \\ &= Q_{out}(T) - Q_{out}(T=0) + \Delta B \\ &= Q_{eff}(T) - Q_{out}(T=0) \\ &= TKE(T) - TKE(T=0). \end{aligned} \quad (8)$$

Eq. (8) means that one can also write

$$\begin{aligned} Q_{eff}(T) &= TKE(T) \\ &= Q_{out}(T=0) + E_x \\ &= TKE(T=0) + E_x, \end{aligned} \quad (9)$$

which is what one observes experimentally i.e. the fragments in the ground state with $Q_{out}(T=0)$ ($=TKE(T=0)$) and light particle(s) and γ -rays of energy E_x . The remaining excitation energy of the decaying system is then,

$$E_{CN}^* - E_x = |Q_{out}(T)| + TKE(T=0) + TXE(T), \quad (10)$$

which again shows that the exit channel fragments are obtained with their TKE in the ground-state, i.e. with $TKE(T=0)$. The excitation energy $TXE(T)$ in (10) is used in the secondary emission of light particles from the fragments, which are not treated here. Instead, we compare our calculations with the primary pre-secondary-evaporation fragments emission data.

We notice from Eq. (7) that for the ground-state ($T=0$) decay,

$$Q_{eff}(T=0) = Q_{out}(T=0) = TKE(T=0), \quad (11)$$

as is the case for exotic cluster radioactivity [21,38]. In fact, one can write Eq. (7) as

$$Q_{eff}(T) = Q_{out}(T) + \Delta B, \quad (12)$$

where

$$\Delta B = [B_1(T) + B_2(T)] - [B_1(T=0) + B_2(T=0)], \quad (13)$$

the difference of binding energies at temperature T and the ground-state binding energies of the two fragments. Also, for the ground-state ($T=0$) decays, according to Eq. (8), $E_x = 0$ (no particle or γ -ray emission), as is known to be true for exotic cluster radioactivity [21,38].

Thus, at temperature T , the preformation factor P_0 in Eq. (5) is calculated at $R_a = C_t(\eta) + \overline{\Delta R}$, with the temperature effects also included in $\psi(\eta)$ through a Boltzmann-like function

$$|\psi|^2 = \sum_{\nu=0}^{\infty} |\psi^\nu|^2 \exp(-E^\nu/T), \quad (14)$$

with the compound nucleus temperature T (in MeV) related as

$$E_{CN}^* = (A/9)T^2 - T; \quad (15)$$

and for the penetrability P , Eqs. (6) and (7) for each η and T -values, mean that

$$V(R_a) = V(C_t + \overline{\Delta R}) = V(R_b) = Q_{eff}(\overline{\Delta R}) = TKE(T), \quad (16)$$

with R_b as the second turning point, and penetrability P calculated as the WKB tunnelling probability for the path shown in Fig. 1 (or Fig. 8), as

$$P = \exp\left[-\frac{2}{\hbar} \int_{R_a}^{R_b} \{2\mu[V(R) - Q_{eff}]\}^{1/2} dR\right], \quad (17)$$

solved analytically [18].

The fragmentation potential $V_R(\eta, T)$ at any temperature T , in Eq.(4), is calculated within the Strutinsky renormalization procedure, as

$$V_R(\eta, T) = \sum_{i=1}^2 [V_{LDM}(A_i, Z_i, T)] + \sum_{i=1}^2 [\delta U_i] \exp\left(-\frac{T^2}{T_0^2}\right) + E_c(T) + V_P(T) + V_\ell(T), \quad (18)$$

where the T -dependent liquid drop energy $V_{LDM}(T)$ is that of Ref. [29] with the (Seeger's) constants at $T=0$ re-fitted to give the experimental binding energies B [31], defined as $B = V_{LDM}(T = 0) + \delta U$. The shell corrections δU are calculated in the "empirical method" of Myers and Swiatecki [40]. Some of these details are given in Appendix I. Figure 2 illustrates the kind of comparisons obtained for $V(\eta)$ calculated at $R = C_1 + C_2 = C_t$ and $T=0$ for the experimental and newly fitted binding energies. Apparently, the binding energies fit within 1 to 1.5 MeV.

The V_P is an additional attraction due to the nuclear proximity potential [41], which is also considered temperature-dependent here,

$$V_P(R, T) = 4\pi\bar{R}(T)\gamma b(T)\Phi(s, T), \quad (19)$$

where $\bar{R}(T)$ and $\Phi(s, T)$ are, respectively, the inverse of the root mean square radius of the Gaussian curvature and the universal function which is independent of the geometry of the system, given by

$$\Phi(s, T) = \begin{cases} -\frac{1}{2}(s - 2.54)^2 - 0.0852(s - 2.54)^3 & \text{for } s \leq 1.2511 \\ -3.437\exp\left(-\frac{s}{0.75}\right) & \text{for } s \geq 1.2511 \end{cases} \quad (20)$$

$$\bar{R}(T) = \frac{C_1(T)C_2(T)}{C_t(T)}, \quad (21)$$

and γ is the specific nuclear surface tension given by

$$\gamma = 0.9517 \left[1 - 1.7826 \left(\frac{N - Z}{A} \right)^2 \right] \text{MeVfm}^{-2}. \quad (22)$$

In Eq. (20), $s(T) (= \frac{R - C_t(T)}{b(T)})$ is the overlap distance, in units of b , between the colliding surfaces. The temperature dependence in radii R_i is given as [29,32],

$$R_i(T) = r_0(T)A_i^{\frac{1}{3}} = 1.07(1 + 0.01T)A_i^{\frac{1}{3}} \quad (23)$$

with the surface width

$$b(T) = 0.99(1 + 0.009T^2). \quad (24)$$

The same temperature dependence of $R(T)$ is also used for Coulomb potential $E_c(T) = Z_1Z_2e^2/R(T)$, where the charges Z_i are fixed by minimizing the potential $V_R(\eta, T)$ in the charge asymmetry coordinate $\eta_Z =$

$(Z_1 - Z_2)/(Z_1 + Z_2)$. The shell corrections δU in Eq. (18) are considered to vanish exponentially for $T_0 = 1.5$ MeV [42].

Also, for the angular momentum effects (so far included here for the calculation of total kinetic energy only)

$$V_\ell(T) = \frac{\hbar^2 \ell(\ell + 1)}{2I(T)}. \quad (25)$$

In the non-sticking limit, where $R_a = C_1(T) + C_2(T) + \Delta R = C_t(T) + \Delta R$, the moment of inertia in (25) is given by

$$I(T) = I_{NS}(T) = \mu R_a^2. \quad (26)$$

In this case, the separation distance ΔR is assumed to be beyond the range of nuclear proximity forces, which is about 2 fm. However, when ΔR is within the range of nuclear proximity (< 2 fm), we get in the complete sticking limit

$$I(T) = I_S(T) = \mu R_a^2 + \frac{2}{5} A_1 m C_1^2 + \frac{2}{5} A_2 m C_2^2. \quad (27)$$

For the ℓ -value, in terms of the bombarding energy E_{cm} of the entrance channel η_{in} , we have

$$\ell = \ell_c = R_a \sqrt{2\mu[E_{cm} - V(R_a, \eta_{in}, \ell = 0)]}/\hbar, \quad (28)$$

or, alternatively, it could be fixed for the vanishing of fusion barrier. In this work, however, we use $\ell = 0$ for the IMF cross sections and take ℓ_c as a variable parameter for total kinetic energy (TKE) calculations (see Fig. 8).

The mass parameters $B_{\eta\eta}(\eta)$, representing the kinetic energy part in Eq. (4), are the smooth classical hydrodynamical masses [43], since we are dealing here with a situation where the shell effects are almost completely washed out.

The assault frequency ν_0 , in Eq.(2), is given simply as

$$\nu_0 = \frac{(2E_2/\mu)^{1/2}}{R_0}, \quad (29)$$

with the kinetic energy of the lighter fragment $E_2 = (A_1/A)Q_{eff}$, for the Q_{eff} shared between the two fragments as inverse of their masses. However, for the calculations of s-wave cross sections, instead of ν_0 , we use an empirically determined normalization constant.

Finally, the temperature dependent scattering potential $V(R,T)$, normalised to the exit channel binding energy, is

$$V(R, T) = Z_1 Z_2 e^2 / R(T) + V_P(T) + V_\ell(T). \quad (30)$$

This means that all energies are measured w.r.t $B_1(T) + B_2(T)$, and the fragments go to ground state ($T \rightarrow 0$) via the emission of light particle(s) and/or γ -rays of energy E_x .

III. CALCULATIONS

The calculations are made in two steps: (i) with temperature effects included only in the shell corrections, i.e., using $\delta U(T)$, but T-independent V_{LDM} and $V(R)$; and (ii) with temperature effects included also in both the liquid drop energy and scattering potential, i.e., using $V_{LDM}(T)$, $\delta U(T)$ and $V(R,T)$. This allows us to study explicitly the role of temperature in different terms of the potential. In both sets of the calculations, we first take $\ell=0$, i.e., use $V_\ell=0$ through out, but then study the effect of adding this term to the potential $V(R)$ for calculating the total kinetic energy (TKE) alone.

A. Temperature effects only in shell corrections

Figure 3 gives our calculated fragmentation potentials $V(\eta, T)$ for $^{56}Ni^*$ at $T=0$, as well as at other two temperatures referring to the compound nucleus excitation energies E_{CN}^* of the experiments of Ref. [2,3]. The R-values chosen are: $R = R_a = C_t$ at $T=0$, and, as before [16], $R = R_a + \overline{\Delta R}$ with $\overline{\Delta R} = 0.30$ and 0.31 fm, arbitrarily, for $T = 3.39$ and 3.60 MeV which correspond to the experimental energies $E_{cm} = 51.6$ and 60.5 MeV, respectively. The near independence of the structure in $V(\eta)$ on R-value was studied in our earlier works [21,28]. The δU at these temperatures reduce

almost to zero. However, we notice that the $N=Z$, $A=4n$ α -nucleus structure is obtained at all temperatures, which has its origin apparently in the macroscopic liquid drop energy and is due to the "Wigner term" in it, as was also shown earlier in Refs. [15,16]. Note that here the V_{LDM} and other R -dependent terms (E_c and V_P) are not yet T -dependent (see next subsection). This means that for use of only δU as T -dependent, the $N=Z$ α -nuclei fragments should be produced preferentially in the decay of $^{56}Ni^*$ at all temperatures.

The preformation probability P_0 of the fragments, calculated for the potentials in Fig. 3, is given in Fig. 4. The case of $T = 0$ is not shown here since cold ^{56}Ni (in the ground-state) can not decay because of its negative Q -value. Interesting enough, for both the temperatures (the two temperatures are nearly the same), the yields are large for only a small window of $A \leq 16$ fragments, including the light particles ($A \leq 3$). Also, the α -nucleus fragments 4He , 8Be , ^{12}C and ^{16}O and the light particle 1H (in addition to the evaporation residues, not included here) are preferentially preformed. This means that, out of all the fragments observed in the decay of $^{56}Ni^*$, the ones with $A \leq 16$ are strongly preformed. The other ones with $A > 16$, if observed, must have larger penetrability P , since the decay constant is a combined effect of both the preformation factor P_0 and penetrability P (ν_0 is nearly constant).

Figure 5 gives the results of our calculation for the normalized decay constants, equivalently, the s -wave production cross sections for *only* the most favoured (largest yields or cross sections) α -nucleus fragments, compared with the experimental data at two energies, taken from Fig. 9 of Ref. [3]. In the lower panel, the calculation at $E_{cm}=51.6$ MeV, using $\overline{\Delta R}=0.3$ fm, is fully normalized to the experimental data for the favoured α -nucleus fragments only. Then, in the upper panel, for the higher energy $E_{cm}=60.5$ MeV we find that, for the use of the same normalization as obtained in lower panel and for a further normalization of the $A=12$ fragment yield, the best fit to the α -nuclei fragment data is obtained for $\overline{\Delta R}=0.29$ fm, a value lower than that used for the lower incident energy $E_{cm}=51.6$ MeV. This is contrary to the expected behaviour of increased R at higher temperatures but, as we shall see below in Fig. 7, this is a result of our having not included here the contribution of angular momentum term in the fragmentation potential ($V_\ell = 0$ in $V(\eta, T)$) and hence in the cross sections. Also, the inclusion of temperature effects in other terms (the V_{LDM} , E_c and V_P) are important, as is shown below in subsection III.B. Hence, Fig. 5 (and Fig. 7 below) show that the dynamical cluster-decay model contains the required structure of the measured yields (and TKEs) in this experiment [2,3].

Figure 6 shows the complete mass spectra for decay of $^{56}Ni^*$ calculated at both the energies and compared with the measured yields [3]. The calculated yields are for the energetically favoured, most probable, mass fragments (see Figs. 3 and 4). Note that the experimental data in [2,3] are available only for fragments heavier than mass 11, and in steps of mass one for $E_{cm}=60.5$ MeV, but in steps of only mass two for $E_{cm}=51.6$ MeV due to a deteriorated mass resolution at the lower bombarding energy. For comparisons, the calculations are normalized to the experimental data for one fragment mass ($A=20$) only. The role of the penetrability P is evident in this figure, since some of the strongly preformed fragments, like 4He and 1H in Fig. 4, are now shown as less favoured decays (smaller cross sections, not shown in Fig. 6 since they lie below the chosen scale). The same is true of weakly preformed fragments (in Fig. 4), with $A > 16$. Specifically, amongst the light particles, mass 3 fragment (3He) is shown to be produced with a large cross section, and for lighter fragments ($A < 12$), instead of $A=8$ (8Be), the fragments with $A=6$ and 10 are shown to be produced with larger cross sections. This means that of all the residue products ($A \leq 4$, not studied here) only mass 3 fragment (3He) is produced and that the mass 4 (4He) fragment is not at all produced as a dynamical cluster-decay fragment. This non-occurrence of 4He as a dynamical cluster-decay product, is an interesting result, giving a strong support to the credential of the model. For mass 8 (Be) decay, perhaps the contribution of higher ℓ -values is important. For the heavier fragments ($A > 20$), the calculated cross sections are rather small due to the fact that here the contribution of only $\ell = 0$ term is considered. Also, in experiments it is difficult to separate the contributions of direct (such as alpha-transfer and orbiting processes) and compound nucleus yields for the heavy mass fragments ($A > 20$) (see Ref. [1] and references therein). Thus, in view of the fact that we are dealing here with only the $\ell = 0$ case and that the temperature effects are not included in full in the potential, the comparisons in Fig. 6 between the theory and experiments could be said atleast reasonable.

Figure 7 shows the results of our calculation for total kinetic energy (TKE), with angular momentum ℓ effects included only in the scattering potential $V(R)$. We notice that the calculated TKEs for the sticking limit (using I_S) compare reasonably good with the experimental data. This means that, even though $\overline{\Delta R}$ is non-zero ($=0.29$ and 0.3 fm), the sticking limit for the moment of inertia is preferred. Also, unlike the $\overline{\Delta R}$ -values, the ℓ -values required for the case of higher energy data is now of a larger value ($\ell = 25\hbar$ for $E_{cm} = 60.5$ MeV as compared to $24\hbar$ for $E_{cm} = 51.6$ MeV), as expected. The measured TKEs are taken from Ref. [3].

B. Fully temperature-dependent potential

Figure 8 shows the scattering potential $V(R, T, \ell)$ for temperature effects included in all the terms of the potential (compare this figure for $\ell = 0$, with Fig. 1 where temperature effects are included in δU only). Notice that as ℓ -value

increases, the $\text{TKE}(\overline{\Delta R})$ -value increases, since the decay path for all the ℓ -values begins at $R = R_a$. Figure 9 gives our calculated fragmentation potentials $V(\eta, T)$. The T-values chosen are the same as in Fig. 3, where temperature effects were included only in the shell corrections. The R-values here are: $R(T) = C_1(T) + C_2(T) + \overline{\Delta R} = C_t(T) + \overline{\Delta R}$, with $\overline{\Delta R}$ -values as shown in the figure. We notice in Fig. 9 that, due to the inclusion of temperature effects in all terms, the minima in the potential, which were earlier only for α -nuclei, are now obtained for both the α and non- α fragments. This happens, possibly, due to the pairing energy term $\delta(T)$ in formula (32) of Davidson et al. [29], which goes to zero for $T > 2$ MeV. Thus, with the addition of temperature, not only the shell structure effects go to zero but also the explicitly preferred α -nucleus structure washes out. Also, we notice that the light particles ($A \leq 4$) structure changes; in particular, the minimum at ${}^4\text{He}$ disappears and a shallow minimum at ${}^2\text{H}$ appears.

Figure 10 gives the preformation factors P_0 for the two experimentally chosen temperatures only, since the ground-state (T=0) decay is not possible. We notice that the formation yields are large only for light fragments ($A < 16$) and are of the same orders as in Fig. 4, except that now the non- α fragments are also preformed equally strongly. However, the calculated decay constants, equivalently, the fragments (s-wave) production cross sections, in Fig. 11 do not show much improvement in their comparisons with experiments. The comparisons are now somewhat better for the heavier fragments but the yields for fragments lighter than A=9 are very low, lying below the chosen scale. On the other hand, the calculated TKEs in Fig. 12 compare nicely (even better than in Fig. 7) with the experimental data. Only the case of sticking limit is shown since the $\overline{\Delta R}$ -values are still within the proximity limits. Note that the ℓ -dependent contribution is so far added here only in the scattering potential $V(R, T)$ and not yet in the fragmentation potential $V(\eta, T)$ which is needed for both the preformation factor and penetrability. This extension is being carried out.

IV. SUMMARY

In summary, we have reformulated for hot nuclear systems, the preformed cluster-decay model (PCM) of Gupta and collaborators for ground-state decays and applied it for the first time to the decay of a light compound nucleus such as ${}^{56}\text{Ni}^*$ formed in the reaction ${}^{32}\text{S} + {}^{24}\text{Mg}$ carried out at two incident energies $E_{cm}=51.6$ and 60.5 MeV [2,3]. In this experiment, the mass spectra for fragments heavier than mass 12 and the total kinetic energies (TKEs) for only the favoured α -nucleus fragments are measured. Also, at another energy, in between the two above, an enhanced yield is observed for ${}^8\text{Be}$ over the two α -particles emission [7]. Our calculations are made first for the temperature effects included only in shell corrections and then in all terms of the potential, and in each case for $\ell=0$ only. The contribution due to ℓ is added only for estimating the TKEs. Similar to the saddle-point model [11] and/ or the scission-point model [12], the deformations of the fragments are taken into account by the parametrization of the neck-in zone, proposed by Gupta and collaborators [33–35]. This quantity is η -dependent and could be calculated but is taken as a parameter here, which is the only parameter of the model.

For the temperature effects included in shell corrections only, we find that the α -nucleus fragments are favourably preformed and are due to the macroscopic liquid drop energy alone since the shell effects are almost zero at the energies under consideration. The calculated decay constants or the normalized s-wave cross sections, in particular for the α -nucleus fragments are found to contain the complete structure of the experiments for a nuclear shape with fragments separated by about 0.3 fm which is within the limits of nuclear proximity effects. Some of the light particles (other than the ones constituting the evaporation residue, not included here) are also predicted to be there in the mass spectra, but ${}^4\text{He}$ is shown to be absent. With angular moments effects included, the calculated TKEs are found to compare rather nicely with experimental data for the moment of inertia calculated for a sticking limit.

For the full temperature effects in the potential, the non- α fragments are also preformed equally strongly as the α -nucleus fragments. The cluster decay process now occurs at a somewhat larger separation distance, which is also temperature dependent. Hence, the TKEs for a sticking moment of inertia are now in somewhat better agreement with the experiments. However, the comparison between the calculated (s-wave) and measured mass spectra is not improved much, which calls for the inclusion of ℓ -dependent potential in the calculations of yields also, which is underway.

V. APPENDIX I: TEMPERATURE DEPENDENT BINDING ENERGIES

In Eq. (18) we have defined, within the Strutinsky renormalization procedure, the binding energy B of a nucleus at temperature T as the sum of liquid drop energy $V_{LDM}(T)$ and shell correction $\delta U(T)$,

$$B(T) = V_{LDM}(T) + \delta U \exp\left(-\frac{T^2}{T_0^2}\right). \quad (31)$$

The T dependent liquid drop part of the binding energy $V_{LDM}(T)$ used here is that of Davidson et al. [29], based on the semi-empirical mass formula of Seeger [30], as

$$\begin{aligned}
V_{LDM}(T) = & \alpha(T)A + \beta(T)A^{\frac{2}{3}} + \left(\gamma(T) - \frac{\eta(T)}{A^{\frac{1}{3}}} \right) \\
& \times \left(\frac{I^2 + 2|I|}{A} \right) + \frac{Z^2}{r_0(T)A^{\frac{1}{3}}} \left(1 - \frac{0.7636}{Z^{\frac{2}{3}}} \right. \\
& \left. - \frac{2.29}{[r_0(T)A^{\frac{1}{3}}]^2} \right) + \delta(T) \frac{f(Z, A)}{A^{\frac{3}{4}}}, \tag{32}
\end{aligned}$$

where

$$I = a_a(Z - N), \quad a_a = 1,$$

and, respectively, for even-even, even-odd, and odd-odd nuclei,

$$f(Z, A) = (-1, 0, 1).$$

For $T=0$, Seeger [30] obtained the constants, by fitting all even-even nuclei and 488 odd-A nuclei available at that time, as

$$\alpha(0) = -16.11\text{MeV}, \quad \beta(0) = 20.21\text{MeV},$$

$$\gamma(0) = 20.65\text{MeV}, \quad \eta(0) = 48.00\text{MeV},$$

with the pairing energy term

$$\delta(0) = 33.0\text{MeV},$$

from Ref. [44]. Evidently, these constants need be re-fitted since a large amount of data has become available [31], particularly for neutron-rich nuclei. We found that the measured binding energies could be fitted within 1 to 1.5 MeV by changing the bulk constant $\alpha(0)$ and introducing a proton, neutron asymmetry constant a_a . The $\alpha(0)$ works as an overall scaling factor and a_a controls the curvature of the experimental parabola (and hence helps to fit the binding energies for neutron-rich nuclei), as expected. Table 1 gives the new $\alpha(0)$ and a_a constants for all the known nuclei with $1 \leq Z \leq 28$, relevant to present problem. The kind of comparisons obtained between the experimental and calculated binding energies is already illustrated in Fig. 2.

The T -dependent constants in Eq. (32) were obtained numerically by Davidson et al. [29] for the available experimental information on excited states of 313 nuclei in the mass region $22 \leq A \leq 250$ by determining the partition function $\mathcal{Z}(T)$ of each nucleus in the canonical ensemble and making a least squares fit of the excitation energy

$$E_{ex}(T) = V_{LDM}(T) - V_{LDM}(T=0)$$

to the ensemble average

$$E_{ex}(T) = T^2 \frac{\partial}{\partial T} \ln \mathcal{Z}(T).$$

The $\alpha(T)$, $\beta(T)$, $\gamma(T)$, $\eta(T)$ and $\delta(T)$ thus obtained are given in Figure 1 of Ref. [29] for $T \leq 4\text{MeV}$, extrapolated linearly for higher temperatures. For the bulk constant $\alpha(T)$, instead, an empirically fitted expression to a Fermi gas model is used, as

$$\alpha(T) = \alpha(0) + \frac{T^2}{15}.$$

Also, the $\delta(T)$ is constrained to be positive definite at all temperatures, with $\delta(T > 2\text{MeV}) = 0$. Finally, the analytical form for $r_0(T)$, taken from Ref. [45], is

$$r_0(T) = 1.07(1 + 0.01T).$$

For the shell corrections δU in Eq. (31), since there is no microscopic shell model known that gives the shell corrections for light nuclei, we use the empirical formula of Myers and Swiatecki [40]. For spherical shapes,

$$\delta U = C \left[\frac{F(N) + F(Z)}{(A/2)^{\frac{2}{3}}} - cA^{\frac{1}{3}} \right] \quad (33)$$

where

$$F(X) = \frac{3}{5} \left(\frac{M_i^{\frac{5}{3}} - M_{i-1}^{\frac{5}{3}}}{M_i - M_{i-1}} \right) (X - M_{i-1}) - \frac{3}{5} \left(X^{\frac{5}{3}} - M_{i-1}^{\frac{5}{3}} \right) \quad (34)$$

with $X=N$ or Z , $M_{i-1} < X < M_i$ and M_i as the magic numbers 2,8,14 (or 20), 28,50,82,126 and 184 for both neutrons and protons. The constants $C=5.8$ MeV and $c=0.26$. In this paper, we refer to the use of magic numbers 14 or 20 as MS14 or MS20 parametrization.

VI. ACKNOWLEDGMENTS

This work is supported in parts by the Council of Scientific and Industrial Research (CSIR), India, the VW-Stiftung, Germany, and the ULP/IN2P3, France.

- [1] S.J. Sanders, A. Szanto de Toledo, and C. Beck, Phys. Reports **311**, 487 (1999).
- [2] S.J. Sanders, D.G. Kovar, B.B. Back, C. Beck, B.K. Dichter, D. Henderson, R.V.F. Janssens, J.G. Keller, S. Kaufman, T.-F. Wang, B. Wilkins, and F. Videbaek, Phys. Rev. Lett. **59**, 2856 (1987); Phys. Rev. Lett. **61**, 2154 (1988).
- [3] S.J. Sanders, D.G. Kovar, B.B. Back, C. Beck, D.J. Henderson, R.V.F. Janssens, T.F. Wang, and B.D. Wilkins, Phys. Rev. C **40**, 2091 (1989).
- [4] S.J. Sanders, A. Hasan, F.W. Prosser, B.B. Back, R.R. Betts, M.P. Carpenter, D.J. Henderson, R.V.F. Janssens, T.L. Khoo, E.F. Moore, P.R. Wilt, F.L.H. Wolfs, A.H. Wuosmaa, K.B. Beard, and Ph. Benet, Phys. Rev. C **49**, 1016 (1994).
- [5] R. Nouicer, C. Beck, R.M. Freeman, F. Haas, N. Aissaoui, T. Bellot, G. de France, D. Disdier, G. Duchêne, A. Elanique, A. Hachem, F. Hoellinger, D. Mahboub, V. Rauch, S.J. Sanders, A. Dummer, F.W. Prosser, A. Szanto de Toledo, S.L. Cavallaro, E. Uegaki, and Y. Abe, Phys. Rev. C **60**, 041303 (1999).
- [6] C. Beck, R. Nouicer, D. Disdier, G. Duchêne, G. de France, R.M. Freeman, F. Haas, A. Hachem, D. Mahboub, V. Rauch, M. Rousseau, S.J. Sanders, and A. Szanto de Toledo, Phys. Rev. C **63**, 014607 (2001).
- [7] S. Thummerer, W. von Oertzen, B. Gebauer, S.M. Lenzi, A. Gadea, D.R. Napoli, C. Beck, and M. Rousseau, J. Phys. G: Nucl. Part. Phys. **27**, 1405 (2001).
- [8] C. Bhattacharya, M. Rousseau, C. Beck, V. Rauch, R.M. Freeman, R. Nouicer, F. Hass, O. Dorvaux, K. Eddahbi, P. Papka, O. Stezowski, S. Szilner, D. Mahboub, A. Szanto de Toledo, A. Hachem, E. Martin, and S.J. Sanders, Pramana J. Phys. **57**, 203 (2001); Phys. Rev. C **65**, 014611 (2002).
- [9] R.J. Charity, M.A. McMahan, G.J. Wozniak, R.J. McDonald, L.G. Moretto, D.G. Sarantites, L.G. Sobotka, G. Guarino, A. Pantaleo, F. Fiore, A. Gobbi, and K.D. Hildenbrand, Nucl. Phys. A **483**, 43 (1988).
- [10] J. Gomez del Campo, R.L. Auble, J.R. Beene, M.L. Halbert, H.J. Kim, A. D'Onofrio, and J.L. Charvet, Phys. Rev. C **43**, 2689 (1991); Phys. Rev. Lett. **61**, 290 (1988).
- [11] S.J. Sanders, Phys. Rev. C **44**, 2676 (1991).
- [12] T. Matsuse, C. Beck, R. Nouicer, and D. Mahboub, Phys. Rev. C **55**, 1380 (1997).
- [13] L.G. Moretto, Nucl. Phys. A **247**, 211 (1975).
- [14] R. Vandenbosch and J.R. Huizenga, *Nuclear Fission*, Academic Press, New York 1973.
- [15] M.K. Sharma, R.K. Gupta, and W. Scheid, J. Phys. G: Nucl. Part. Phys. **26**, L45 (2000).
- [16] R.K. Gupta, M. Balasubramaniam, C. Mazzocchi, M. La Commara, and W. Scheid, Phys. Rev. C **65**, 024601 (2002).
- [17] R.K. Gupta, in *Proceedings of the 5th International Conference on Nuclear Reaction Mechanisms*, Varenna, 1988, edited by E. Gadioli (Ricerca Scientifica ed Educazione Permanente, Milano, 1988), p.416.
- [18] S.S. Malik and R.K. Gupta, Phys. Rev. C **39**, 1992 (1989).
- [19] R.K. Gupta, W. Scheid, and W. Greiner, J. Phys. G: Nucl. Phys. **17**, 1731 (1991).
- [20] S. Kumar and R.K. Gupta, Phys. Rev. C **49**, 1922 (1994).
- [21] R.K. Gupta, in *Heavy Elements and Related New Phenomena*, edited by W. Greiner and R.K. Gupta (World Scientific, Singapore, 1999), Vol. II, p. 730.
- [22] R.K. Gupta, D.R. Saroha, and N. Malhotra, J. de Physique Coll. **45**, C6-477 (1984).
- [23] D.R. Saroha, N. Malhotra, and R.K. Gupta, J. Phys. G: Nucl. Phys. **11**, L27 (1985).

- [24] S.S. Malik and R.K. Gupta, J. Phys. G: Nucl. Phys. **12**, L161 (1986).
- [25] R.K. Puri and R.K. Gupta, J. Phys. G: Nucl. Phys. **18**, 903 (1992).
- [26] J. Maruhn and W. Greiner, Phys. Rev. Lett. **32**, 548 (1974).
- [27] R.K. Gupta, W. Scheid, and W. Greiner, Phys. Rev. Lett. **35**, 353 (1975).
- [28] R.K. Gupta and W. Greiner, in Ref. [21], Vol. I, pp. 397, 536.
- [29] N.J. Davidson, S.S. Hsiao, J. Markram, H.G. Miller, and Y. Tzeng, Nucl. Phys. A **570**, 61c (1994).
- [30] P.A. Seeger, Nucl. Phys. **25**, 1 (1961).
- [31] G. Audi and A.H. Wapstra, Nucl. Phys. A **595**, 4 (1995).
- [32] G. Royer, J. Phys. G: Nucl. Phys. **18**, 1781 (1992), and earlier references therein.
- [33] H.S. Khosla, S.S. Malik, and R.K. Gupta, Nucl. Phys. A **513**, 115 (1990).
- [34] R.K. Gupta, S. Kumar, and W. Scheid, Int. J. Mod. Phys. E **6**, 259 (1997).
- [35] S. Kumar and R.K. Gupta, Phys. Rev. C **55**, 218 (1997).
- [36] A. Săndulescu, D.N. Poenaru, and W. Greiner, Sovt. J. Part. Nucl. **11**, 528 (1980).
- [37] H.J. Rose and G.A. Jones, Nature **307**, 245 (1984).
- [38] R.K. Gupta and W. Greiner Int. J. Mod. Phys. E **3**, 335 (1994, Suppl.).
- [39] D.R. Saroha and R.K. Gupta, J. Phys. G: Nucl. Phys. **12**, 1265 (1986).
- [40] W. Myers and W.J. Swiatecki, Nucl. Phys. **81**, 1 (1966).
- [41] J. Blocki, J. Randrup, W.J. Swiatecki, and C.F. Tsang, Ann. Phys. (NY) **105**, 427 (1977).
- [42] A.S. Jensen and J. Damgaard, Nucl. Phys. A **203**, 578 (1973).
- [43] H. Kröger and W. Scheid, J. Phys. G **6**, L85 (1980).
- [44] S. DeBenedetti, *Nuclear Interactions* (John Wiley and Sons, 1964).
- [45] M. Brack and P. Quentin, Phys. Lett. B **52**, 159 (1974).

FIGURE CAPTIONS

- Fig.1 The s-wave ($\ell = 0$) scattering potential for $^{56}Ni^* \rightarrow ^{12}C + ^{44}Ti$, calculated for **no** temperature effects in E_c and V_P , i.e. $V(R) = E_c + V_P$. The Q-values are calculated from T-dependent binding energy $B(T) = V_{LDM} + \delta U(T)$. The actually calculated decay path for $V(R_a) = Q_{eff}(\overline{\Delta R}) = V(C_t(T) + \overline{\Delta R})$ is shown, where $\overline{\Delta R}$ is an average of the separation distances for different fragmentations (different η -values).
- Fig.2 The fragmentation potential for ^{56}Ni at $T=0$, $R = C_t$, using the experimental binding energies (solid squares) [31] and the empirically fitted Seeger's binding energies (solid circles) with the new constants of Table 1. Here, MS14 means the shell corrections from the empirical method of Myers and Swiatecki [40] with Z and N=14 as the magic numbers.
- Fig.3 The fragmentation potentials $V(\eta, R, T)$ for $^{56}Ni^*$ compound system, calculated at the ground-state ($T=0$, $R_a = C_t$) and at various temperatures with $R_a = C_1(T) + C_2(T) + \overline{\Delta R}$ values as shown. The T-dependence is included only in the shell corrections.
- Fig.4 The fragment preformation probability P_0 for $^{56}Ni^*$, calculated by using the fragmentation potentials in Fig. 3 for the two experimental T-values only.
- Fig.5 The calculated s-wave cross sections for the α -nucleus fragments compared with the measured ones produced in the reaction $^{32}S + ^{24}Mg \rightarrow ^{56}Ni^*$ at $E_{cm} = 51.6$ and 60.5 MeV. The data are from Fig. 9 of Ref. [3]. The calculations for $E_{cm} = 51.6$ MeV in the lower panel are made for $\overline{\Delta R} = 0.30$ fm and are normalized completely to the experimental data. Using the same normalization, the calculations for $E_{cm} = 60.5$ MeV in the upper panel are made for $\overline{\Delta R} = 0.29, 0.30$ and 0.31 fm and compared with the experimental data, for a further normalization of the data at fragment mass $A=12$. Only the α -nucleus fragments are studied, since they have the largest cross sections. The dotted lines are drawn only for the guide of eyes.
- Fig.6 Same as for Fig. 5, but studied for all the fragments at $E_{cm} = 51.6$ MeV, $\overline{\Delta R} = 0.30$ fm (upper panel) and $E_{cm} = 60.5$ MeV and $\overline{\Delta R} = 0.29$ fm (lower panel). The calculations are normalized to the experimental data for one fragment mass ($A=20$) only. The calculated (s-wave) cross sections are for the energetically most favoured fragments in η coordinate i.e. fragments lying at the minimum in the fragmentation potential $V(\eta)$, minimized in η_Z coordinate.
- Fig.7 The measured and calculated total kinetic energy (TKE) for average $\overline{\Delta R}$ for the the reaction $^{32}S + ^{24}Mg \rightarrow ^{56}Ni^* \rightarrow A_1 + A_2$, at the two incident energies. The calculations for $\ell \neq 0$ are made for both the cases of sticking and non-sticking limits (see text). The data are from Fig. 5 (summed over all the angles) of Ref. [3]. The same data are also given in Fig. 10 of Ref. [11], where it should be noted that Fig. 10(a) refers to $E_{c.m.} = 60.5$ MeV and Fig. 10(b) to $E_{c.m.} = 51.6$ MeV.
- Fig.8 Same as for Fig. 1, but with ℓ , and T dependences included in E_c and V_P also, i.e., the scattering potential is $V(R, T, \ell) = E_c(T) + V_P(T) + V_\ell(T)$ with Q-value now calculated from $B(T) = V_{LDM}(T) + \delta U(T)$. Only the sticking limit of moment of inertia is used in $V_\ell(T)$. The $T=0$ potential is shown for comparisons. For all ℓ -values, the decay path (dotted line), shown for $\overline{\Delta R}$, begins at $R = R_a$ (marked explicitly). The distribution of energies and definitions of other quantities like ΔB and E_x are indicated for the calculated ΔR -value.
- Fig.9 Same as for Fig. 3, but for T-dependence in all the terms of the fragmentation potential, and at $\overline{\Delta R}$ values as shown.
- Fig.10 Same as for Fig. 4, but for the fragmentation potential of Fig. 9.
- Fig.11 Same as for Fig. 6, but for T-dependence in all the terms of the fragmentation potential, and at $\overline{\Delta R}$ values as shown. For lighter fragments, the calculated yields are not shown as they lie below the chosen scale.
- Fig.12 Same as for Fig. 7, but for T-dependence in all the terms of the fragmentation potential, and at $\overline{\Delta R}$ values as shown.

Table 1. Re-fitted bulk and asymmetry constants for Seeger's mass formula.

Z	N	$\alpha(0)$	a_a	Z	N	$\alpha(0)$	a_a	Z	N	$\alpha(0)$	a_a
1	2	-15.85	0.10	6	9	-15.70	0.10	10	7	-15.70	0.50
	3	-16.95	0.12		10	-15.10	0.10		8	-15.90	0.90
	4	-13.00	0.05		11	-14.80	0.10		13	-15.95	0.50
	5	-13.70	0.12		12,13,15,16	-15.00	0.80		14	-15.70	0.50
2	1	-15.50	0.10		14	-14.85	0.80		9-12,15-22	-16.16	0.88
	2	-16.00	0.10	7	3	-14.30	0.20	11	7	-15.55	0.50
	3	-16.80	0.30		4	-15.20	0.50		8	-15.80	0.50
	4,5	-14.20	0.30		5	-16.20	0.80		14	-15.95	0.50
	6	-13.50	0.10		6	-16.55	0.80		9-13,15-24	-16.20	0.86
	7,8	-13.00	0.10		7	-16.80	0.80	12	8-10	-16.11	0.90
3	1,2,4,5	-16.60	0.10		8	-16.30	0.80		11-25	-16.20	0.86
	3	-16.98	0.98		9	-16.20	0.80	13	8-10	-16.11	0.90
	6	-13.80	0.98		10,11	-15.90	0.94		11-26	-16.22	0.84
	7	-14.30	0.40		12	-15.75	0.94	14	8-12	-16.11	0.90
	8,9	-13.20	0.10		13	-15.80	0.94		13-20,27,28	-16.28	0.84
4	1	-13.00	0.01		14	-15.65	0.94		21-26	-16.22	0.84
	2	-14.50	0.10		15	-15.90	0.94	15	9-13,20-31	-16.30	0.82
	3	-16.20	0.80		16	-16.00	0.94		14-19	-16.36	0.78
	4	-16.98	0.98		17	-16.10	0.93	16	10-14,21-28	-16.30	0.82
	5	-16.70	0.60	8	4	-14.00	0.94		15-20	-16.40	0.78
	6	-15.50	0.80		5	-15.25	0.94		29-33	-16.32	0.80
	7	-15.30	0.50		6	-15.90	0.94	17	11-14,20,21,29-34	-16.36	0.78
	8	-14.30	0.10		7	-16.35	0.94		15-19	-16.45	0.78
	9	-14.00	0.10		8	-16.20	0.94		22-28	-16.32	0.82
	10	-13.30	0.01		9	-16.18	0.94	18	12-14,21,22,31-35	-16.36	0.78
5	2	-14.60	0.10		10	-15.95	0.94		15-20	-16.45	0.78
	3	-16.50	0.10		11	-15.93	0.94		23-30	-16.32	0.78
	4	-16.60	0.60		12,14	-15.85	0.94	19	13,14,22,23,30-36	-16.38	0.78
	5	-16.99	0.10		13	-15.90	0.94		15-21	-16.44	0.78
	6	-16.60	0.60		15	-16.10	0.94		24-29	-16.36	0.80
	7	-16.30	0.10		16	-16.15	0.90	20	14,15,22-37	-16.38	0.78
	8	-15.35	0.10		17	-16.30	0.92		16-21	-16.48	0.78
	9	-15.10	0.10		18	-16.11	0.92	21	15-23,31-38	-16.42	0.77
	10	-14.45	0.10	9	5	-15.25	0.90		24-30	-16.38	0.78
	11	-14.10	0.10		6	-15.90	0.90	22	16-39	-16.42	0.77
	12	-13.45	0.10		7	-16.28	0.90	23	17-40	-16.42	0.77
	13	-13.10	0.10		9	-16.30	0.90	24	18-25	-16.45	0.77
	14	-13.00	0.40		10	-16.15	0.90		26-41	-16.42	0.77
6	2	-13.00	0.10		8,11,17,19,20	-16.20	0.90	25	19-26	-16.46	0.77
	3	-13.85	0.80		12	-16.01	0.90		27-42	-16.42	0.77
	4	-15.70	0.10		13	-16.05	0.90	26	19-43	-16.46	0.77
	5,7	-16.50	0.10		14	-15.95	0.90	27	21-28	-16.48	0.77
	6	-16.65	0.10		15,16,18	-16.11	0.90		29-45	-16.46	0.77
	8	-15.90	0.10	10	6	-15.25	0.50	28	22-48	-16.48	0.77

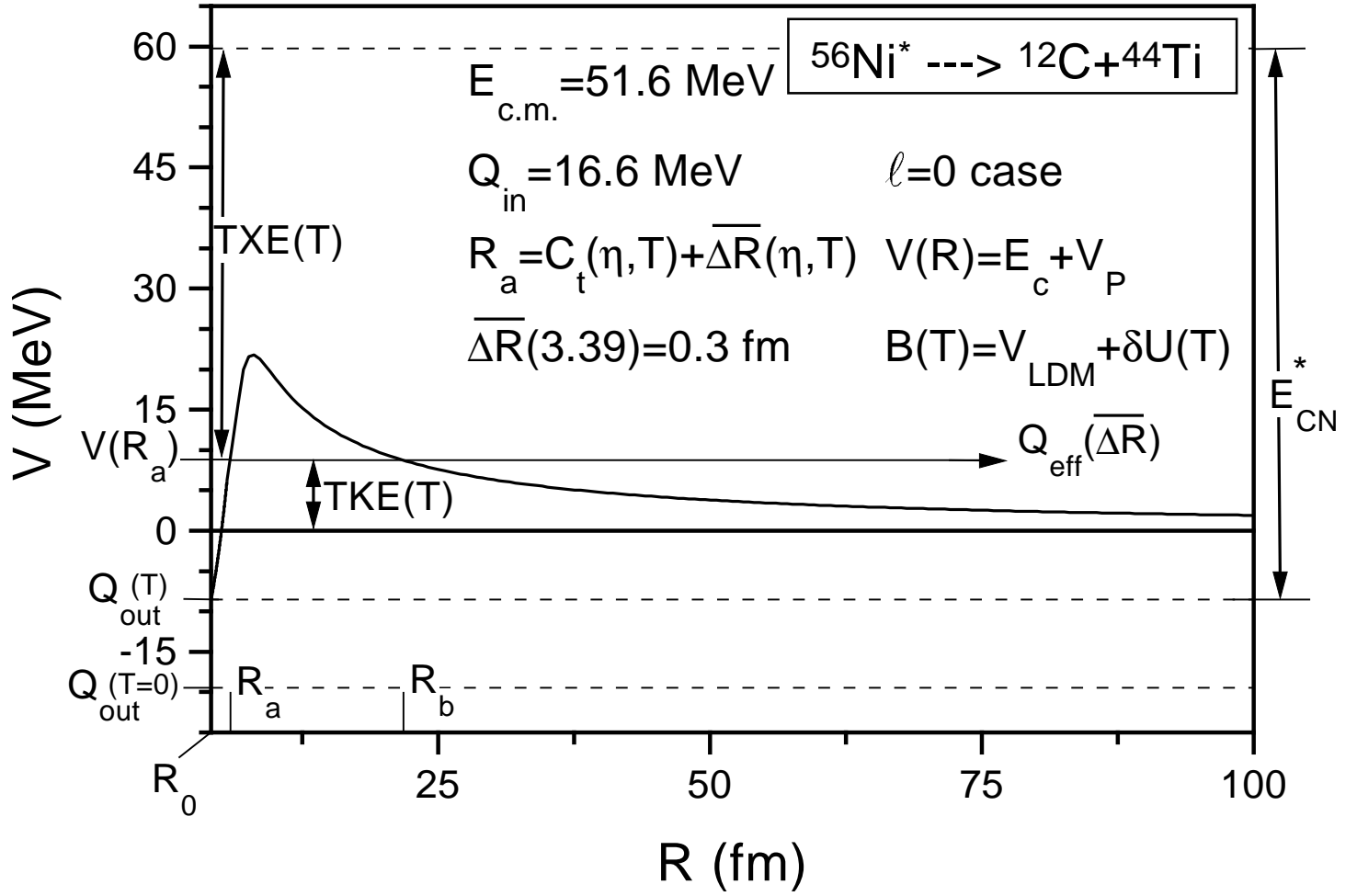


Fig.1 "Cluster decay of hot $^{56}\text{Ni}^*$" - Gupta et al.

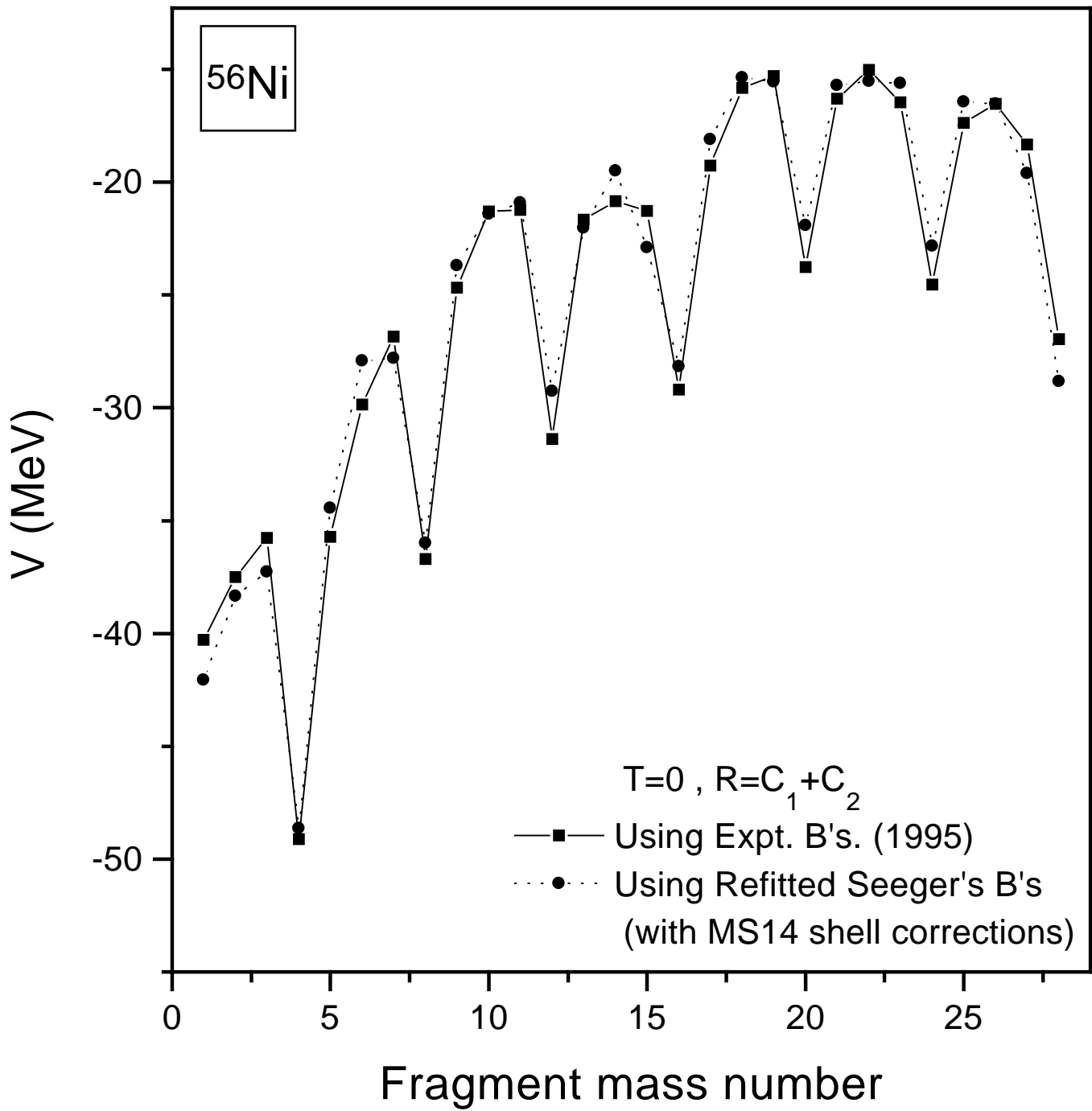


Fig.2 "Cluster decay of hot $^{56}\text{Ni}^*$" - Gupta et al.

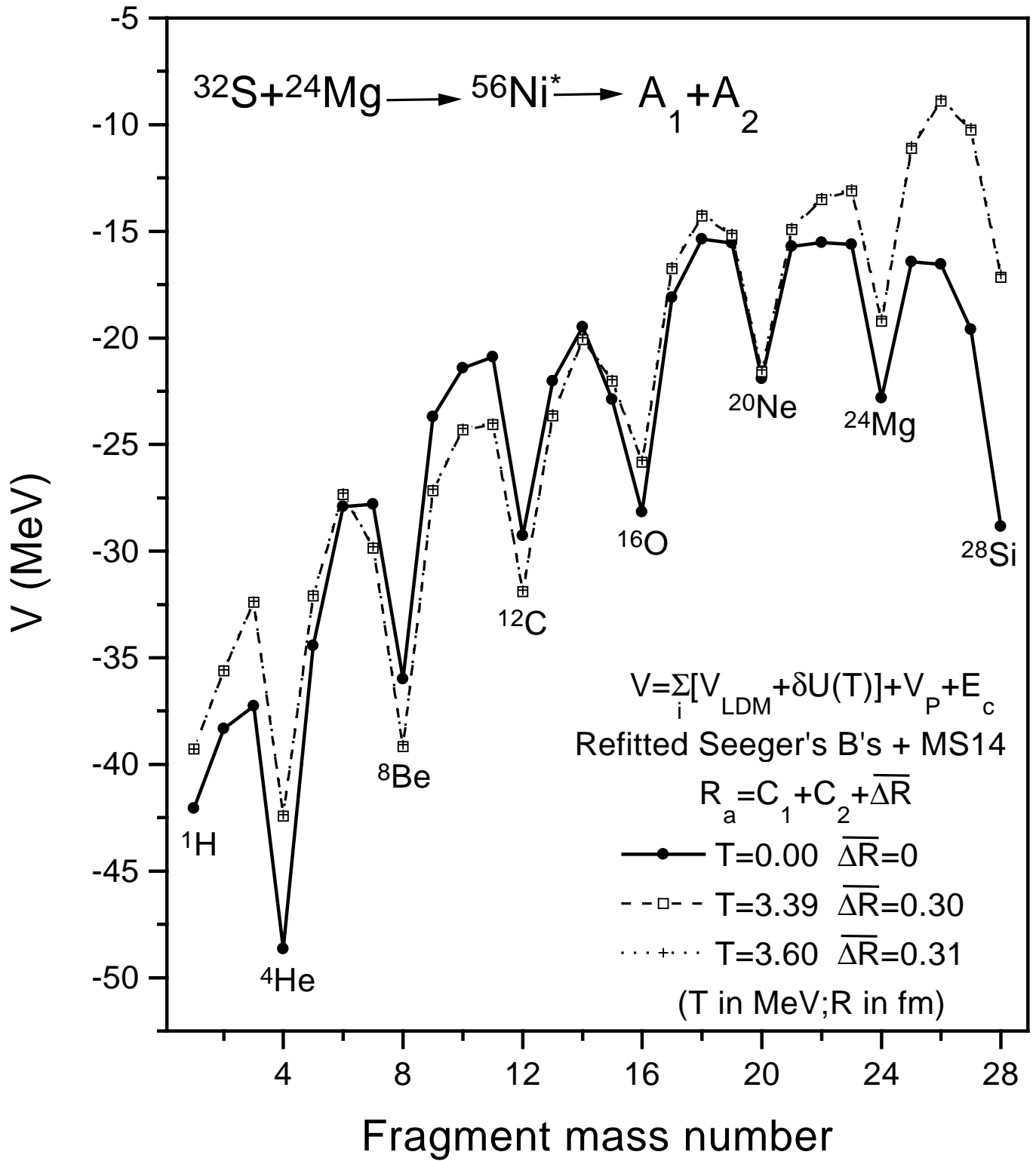


Fig. 3 "Cluster decay of hot $^{56}\text{Ni}^*$" - Gupta et al.

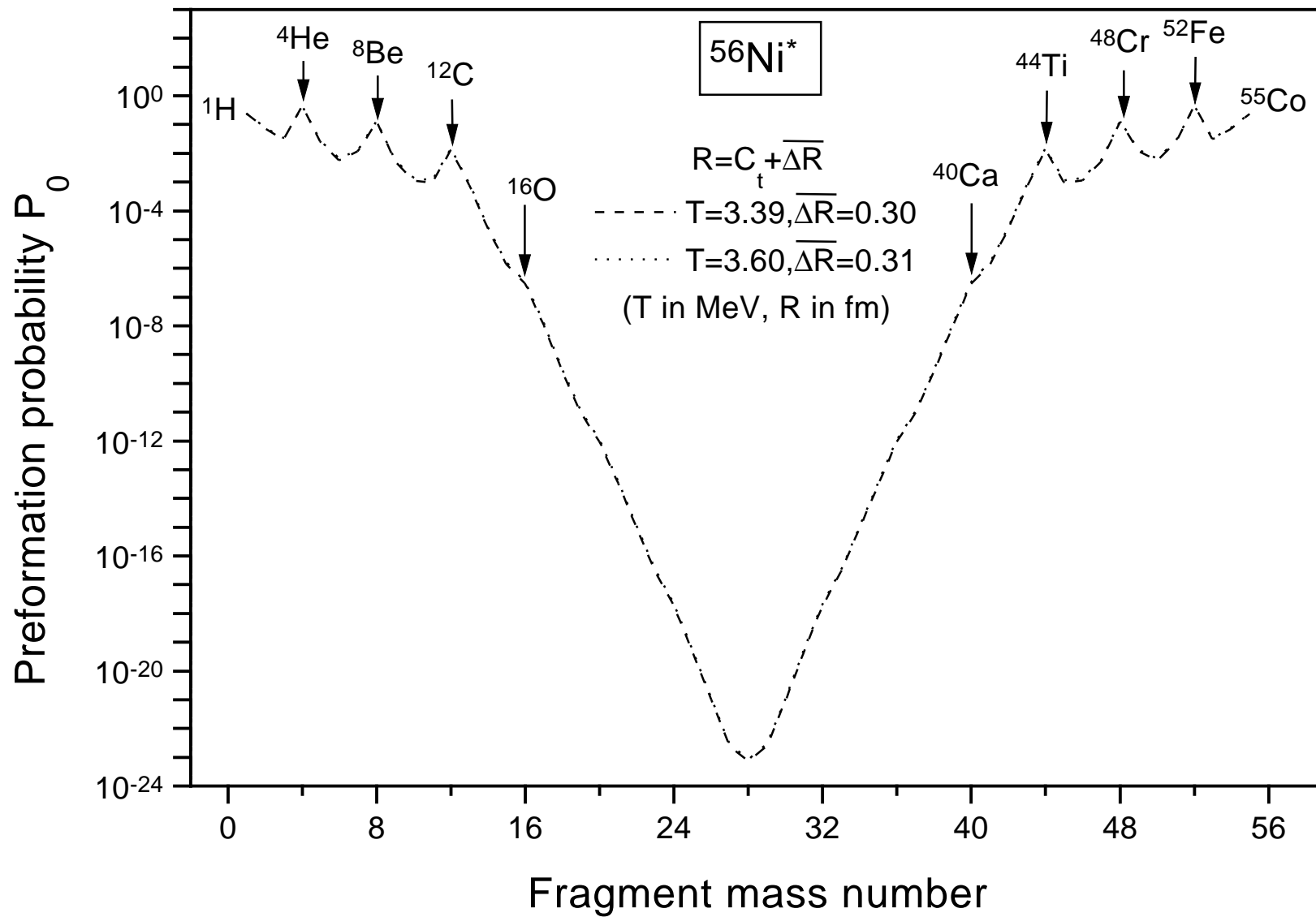


Fig. 4 "Cluster decay of hot $^{56}\text{Ni}^*$" - Gupta et al.

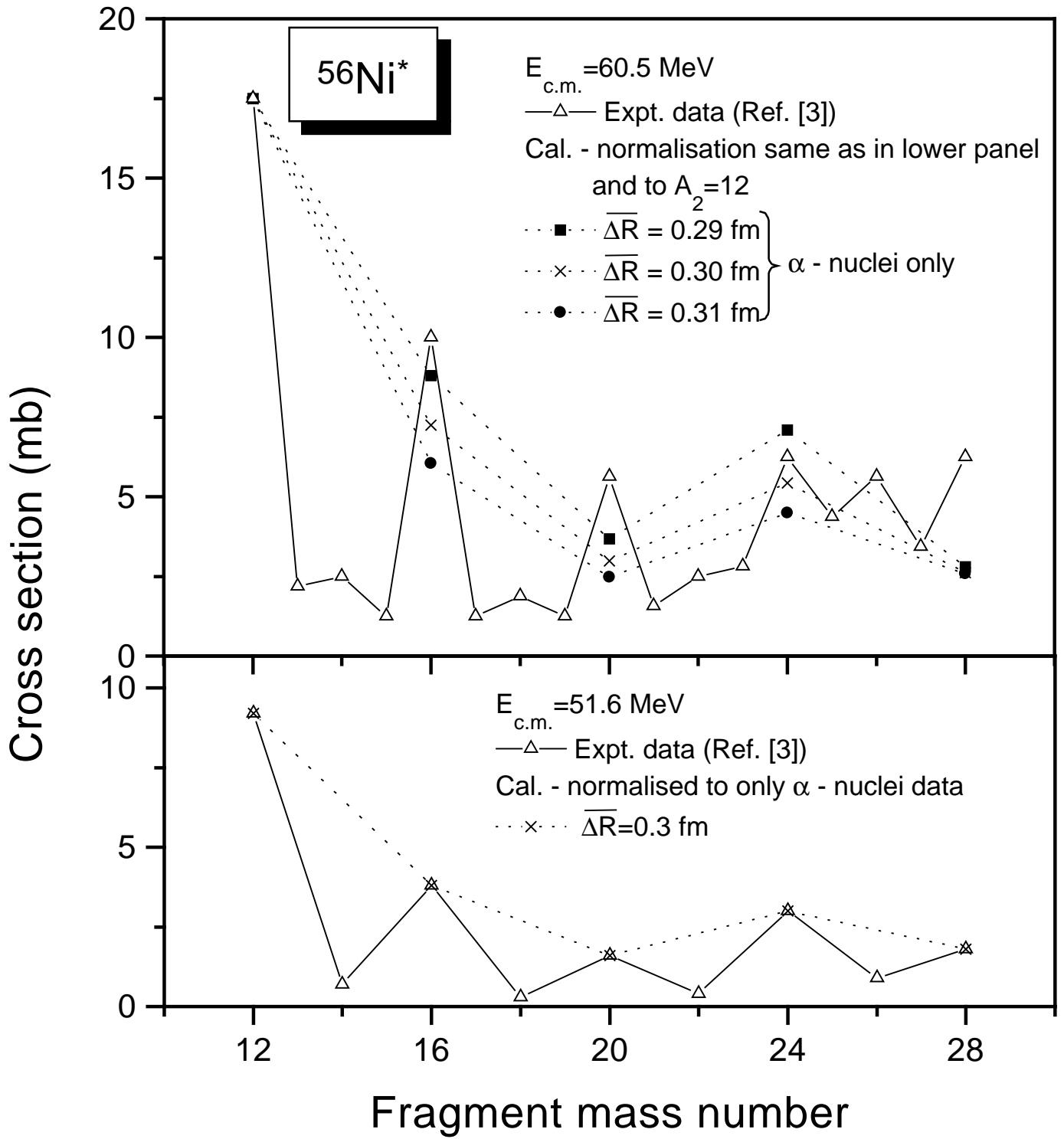


Fig. 5 "Cluster decay of hot $^{56}\text{Ni}^*$" - Gupta et al.

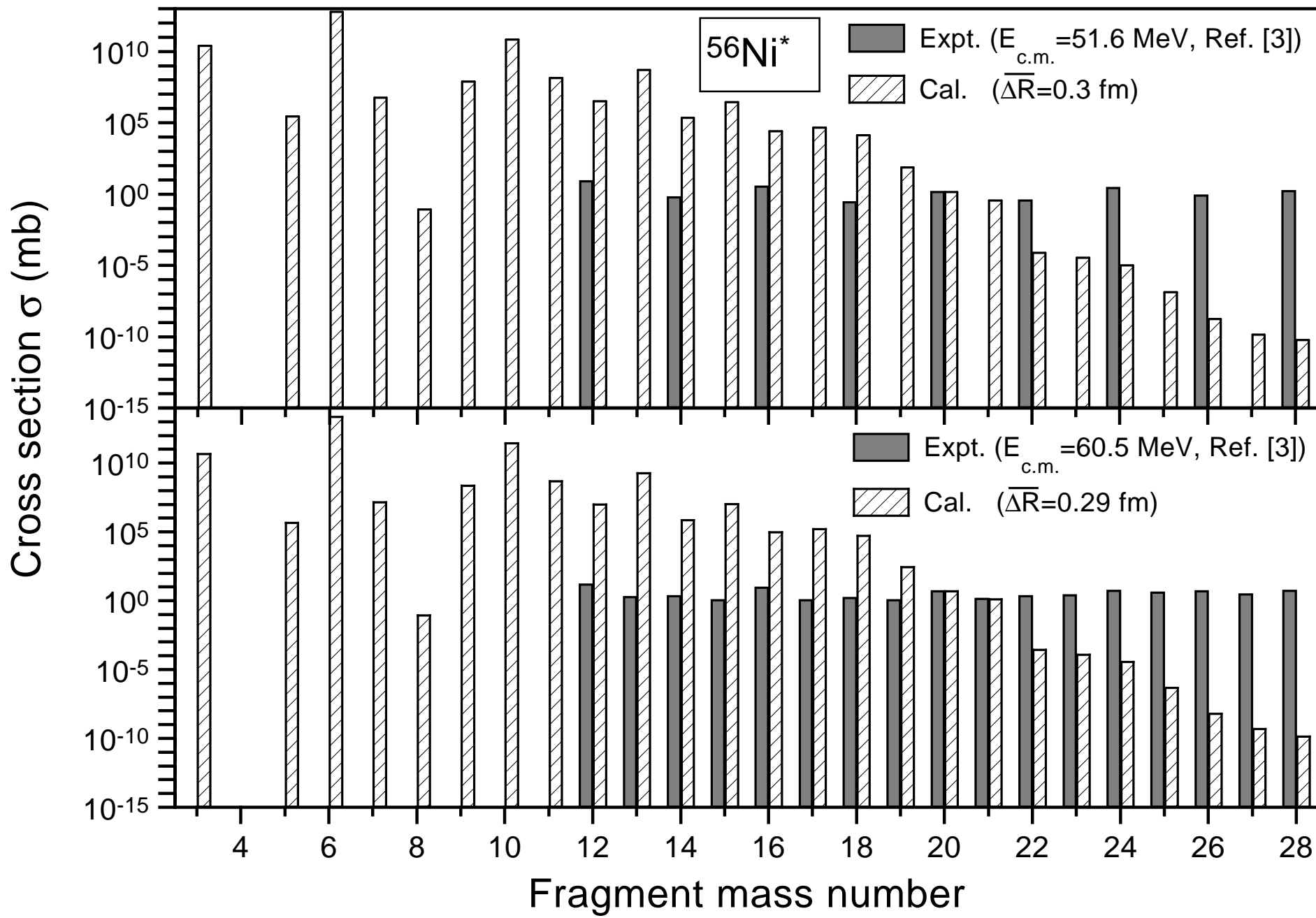


Fig. 6 "Cluster decay of hot $^{56}\text{Ni}^*$" - Gupta et al.

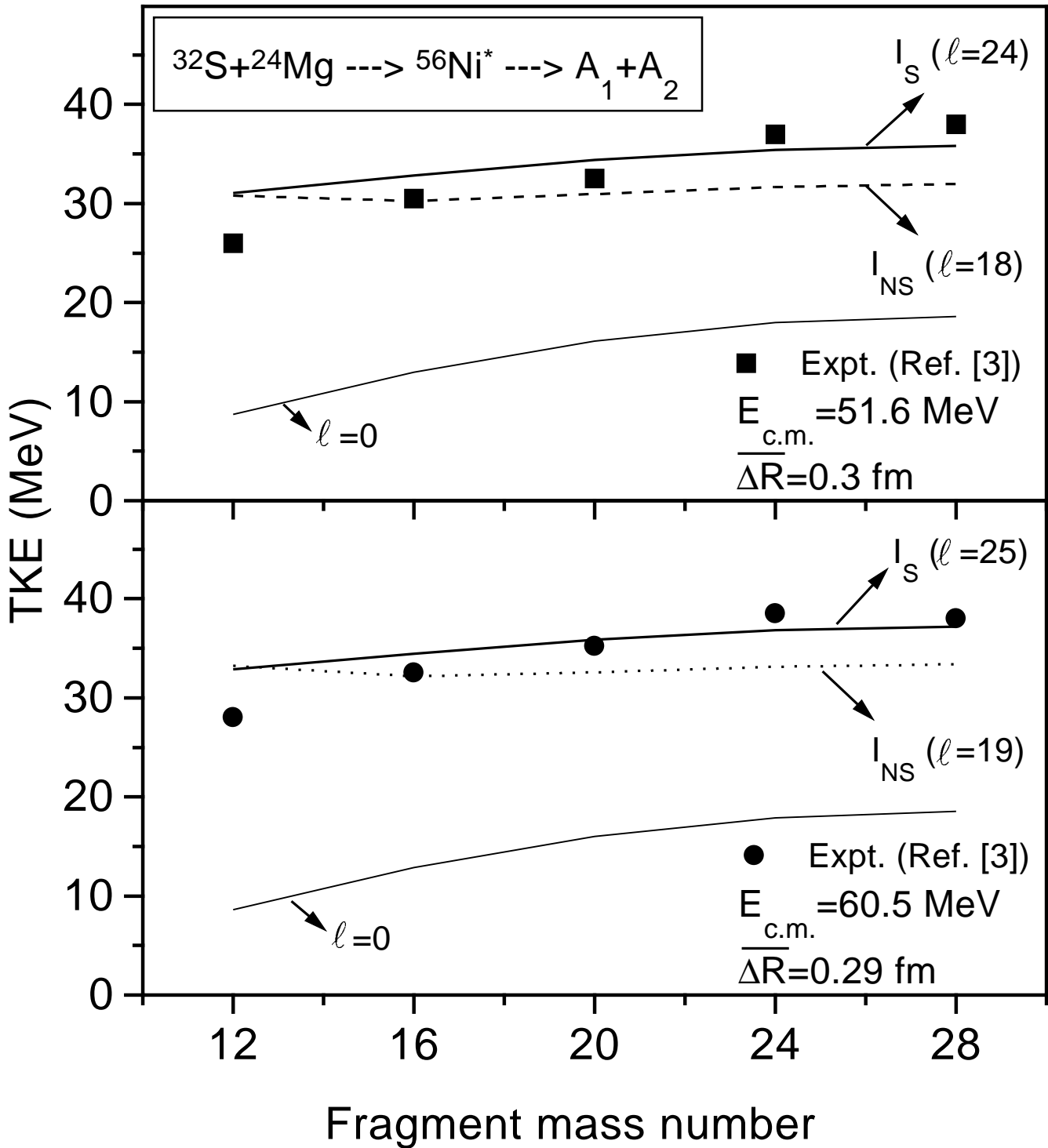


Fig. 7 "Cluster decay of hot $^{56}\text{Ni}^*$" - Gupta et al.

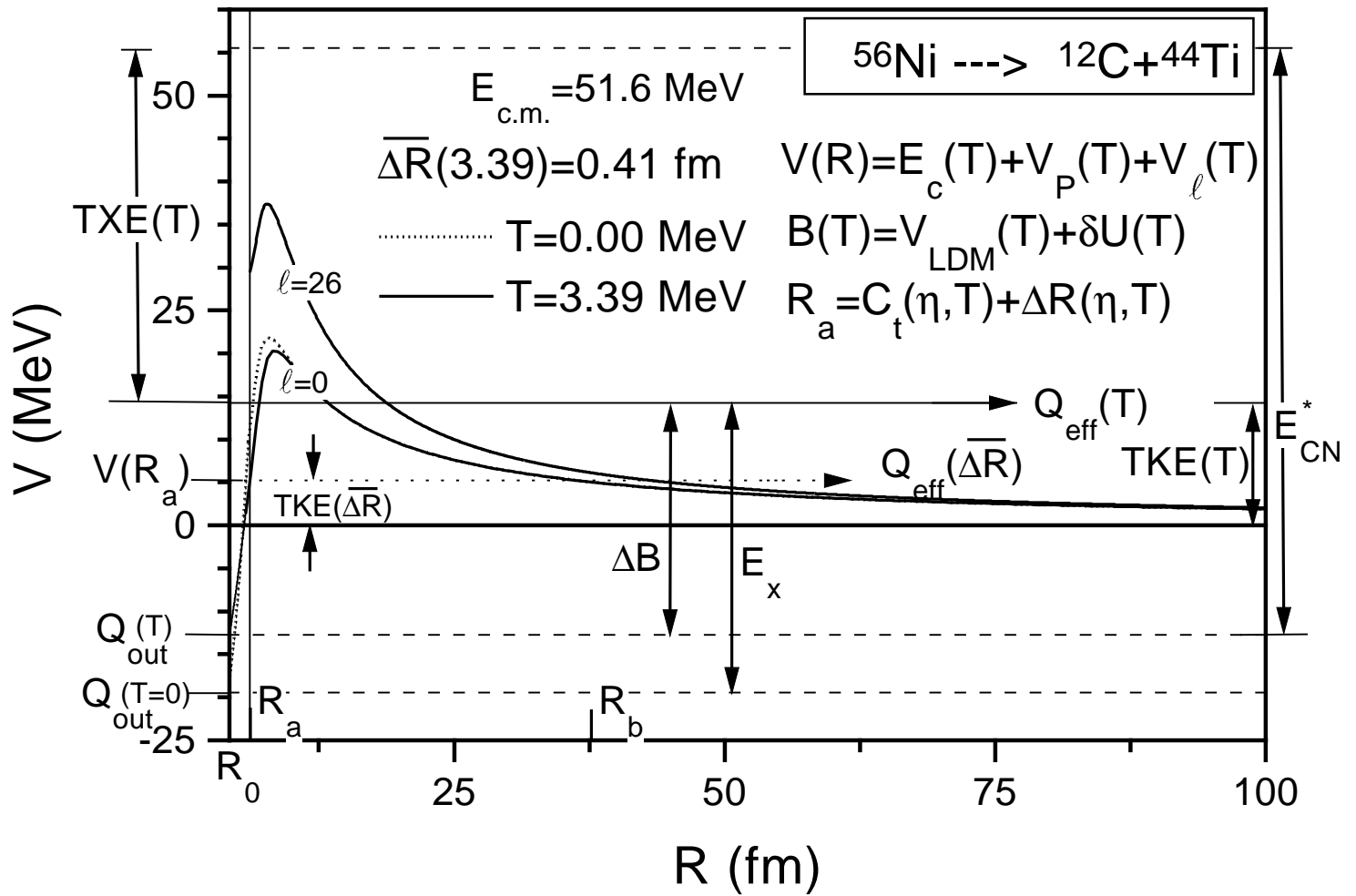


Fig. 8 "Cluster decay of hot $^{56}\text{Ni}^*$" - Gupta et al.

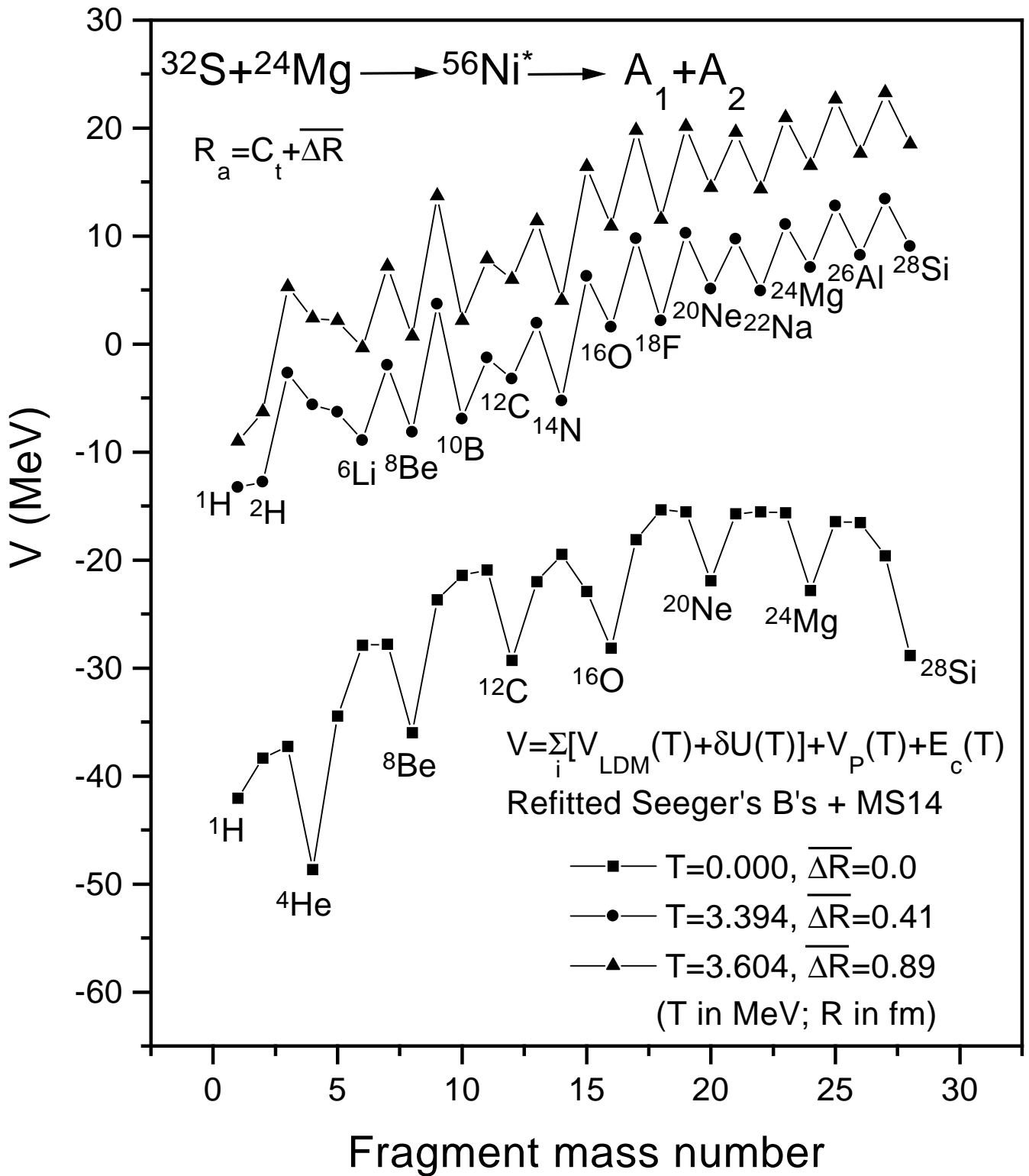
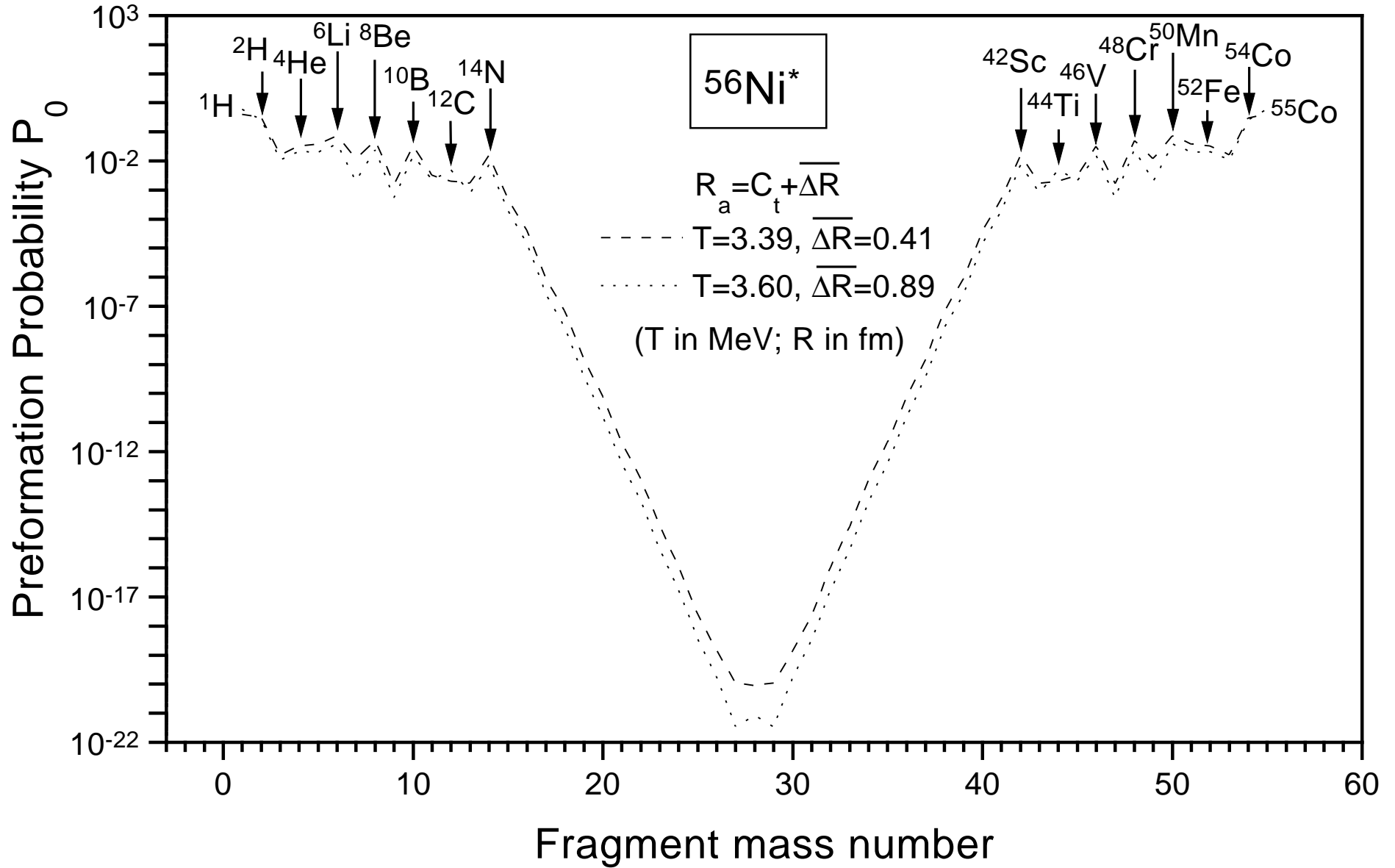


Fig. 9 "Cluster decay of hot $^{56}\text{Ni}^*$" - Gupta et al.

Fig.10 "Cluster decay of hot $^{56}\text{Ni}^*$" - Gupta et al.



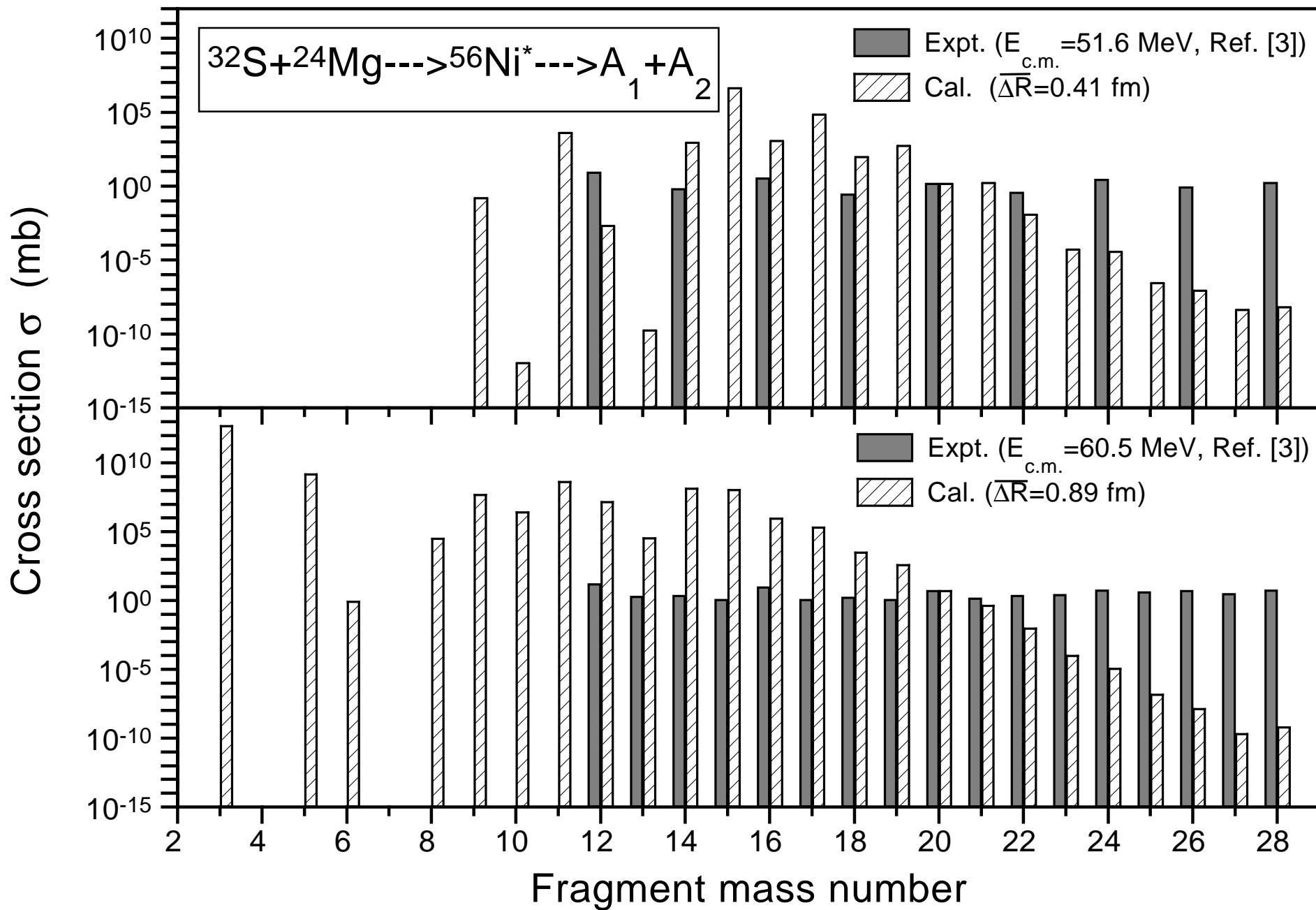


Fig. 11 "Cluster decay of hot $^{56}\text{Ni}^*$..." - Gupta et al.

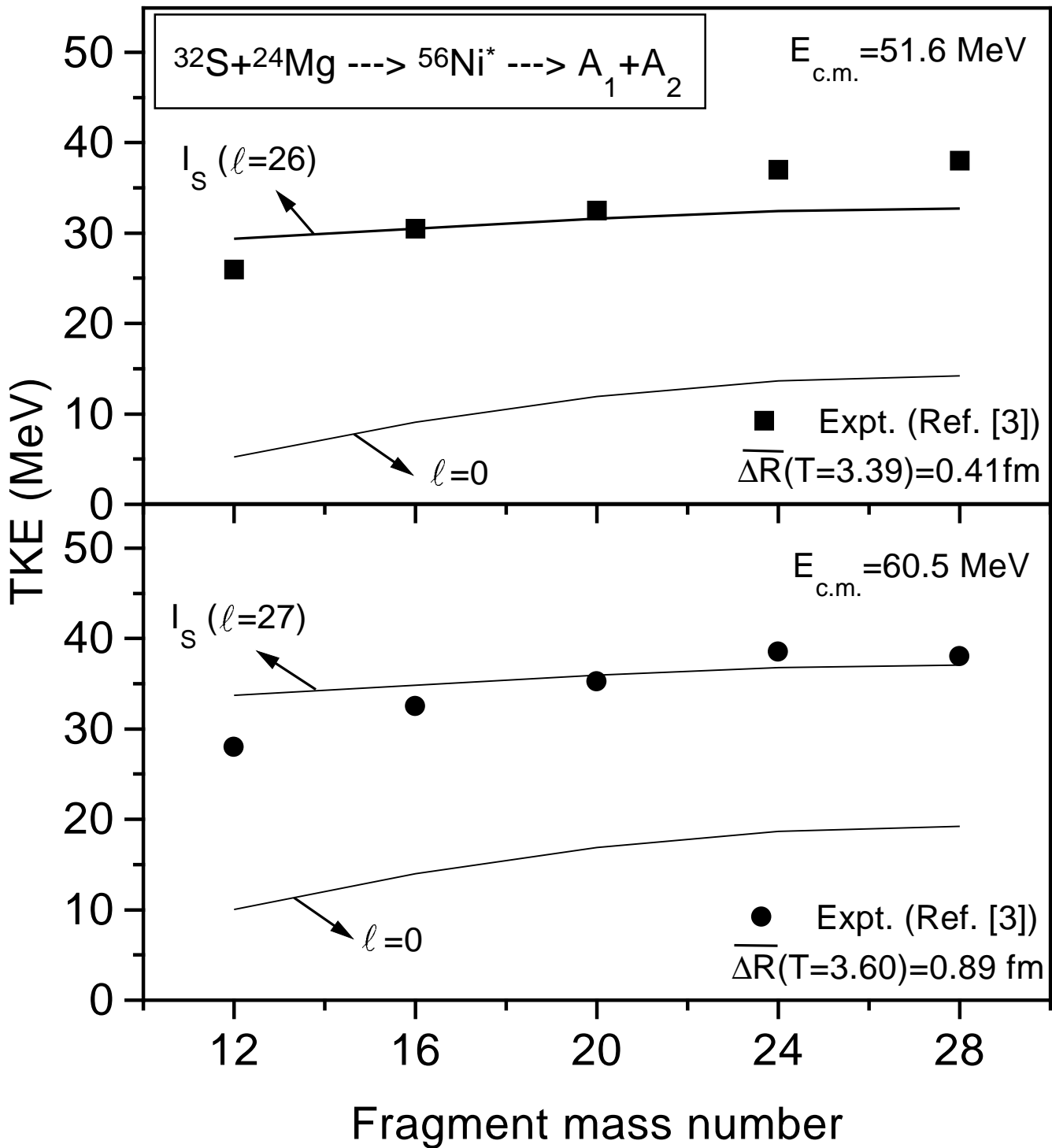


Fig.12 "Cluster decay of hot $^{56}\text{Ni}^*$" - Gupta et al.